

# SUPERCONDUCTING GAMMA-DETECTORS FOR NON-DESTRUCTIVE ANALYSIS IN NUCLEAR SAFEGUARDS

by

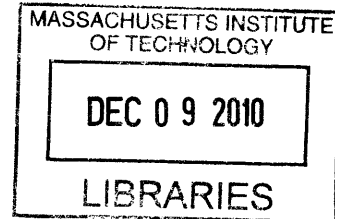
Andrea Elizabeth Robles Olson

**ARCHIVES**

SUBMITTED TO THE DEPARTMENT OF NUCLEAR SCIENCE AND ENGINEERING  
IN PARTIAL FULFILLMENT OF THE REQUIREMENTS FOR THE DEGREE OF

BACHELOR OF SCIENCE IN NUCLEAR SCIENCE AND ENGINEERING  
AT THE  
MASSACHUSETTS INSTITUTE OF TECHNOLOGY

JUNE 2010



© Andrea Elizabeth Robles Olson. All rights reserved.

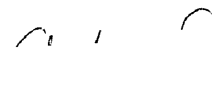
The author hereby grants to MIT permission to reproduce and to distribute publicly paper and electronic copies of this thesis document in whole or in part.

Signature of Author: \_\_\_\_\_


Andrea Elizabeth Robles Olson  
Department of Nuclear Science and Engineering  
May 14, 2010

Certified by: \_\_\_\_\_

  
Richard C. Ewing  
Senior Research Scientist-MIT  
Thesis Supervisor

  
Stephan Friedrich  
Senior Scientist-LLNL  
Thesis Supervisor

Accepted by: \_\_\_\_\_

  
Dennis Whyte  
Associate Professor of Nuclear Science and Engineering  
Chair, NSE Committee for Undergraduate Students

# SUPERCONDUCTING GAMMA-DETECTORS FOR NON-DESTRUCTIVE ANALYSIS IN NUCLEAR SAFEGUARDS

by

Andrea Elizabeth Robles Olson

Submitted to the Department of Nuclear Science and Engineering on May 14, 2010  
In Partial fulfillment of the Requirements for the Degree of  
Bachelor of Science in Nuclear Science and Engineering

## ABSTRACT

Ultra-high energy resolution superconducting gamma ray detectors operated at temperatures of  $\sim 0.1$  K can improve the accuracy of non-destructive analysis of nuclear materials. These detectors offer an order of magnitude improvement in resolution over conventional high-purity germanium detectors. The increase in resolution improves the peak-to-background ratio, and reduces errors from line overlap, therefore allowing the identification of weak gamma rays on top of a high Compton background. The higher resolution also improves the accuracy of isotope ratio measurements in fissile material. In order to understand the spectral background and improve the detector sensitivity, GEANT4 Monte Carlo simulations are used to model the low energy response of these superconducting detectors. The models are used to identify the spectral contributions from Compton scattering and from the detector shielding to assess the feasibility of identifying fissile material in spent nuclear fuel. The detector simulations are compared for accuracy to experimental data. We discuss the superconducting detector model, possible improvements in spectrometer configuration, and their use in nuclear safeguards by the IAEA.

Richard C. Lanza  
Senior Research Scientist-MIT

Stephan Friedrich  
Senior Scientist-LLNL

# TABLE OF CONTENTS

<b>ABSTRACT</b> .....	<b>2</b>
<b>INTRODUCTION</b> .....	<b>4</b>
<b>INTERNATIONAL NUCLEAR SECURITY</b> .....	<b>6</b>
The International Atomic Energy Agency .....	6
The Threat of Nuclear Proliferation .....	7
Safeguarding Techniques .....	8
Non-Destructive Analysis .....	9
Limitations of Current Detector Technologies .....	12
<b>SUPERCONDUCTING DETECTORS</b> .....	<b>13</b>
Detector Components .....	14
Principles of Operation .....	15
Detector Tradeoffs .....	17
Applications of Superconducting Detectors .....	18
<b>SPENT FUEL</b> .....	<b>18</b>
Burnup Calculations .....	19
Detector Technology .....	21
The Spent Fuel Problem .....	21
How can Superconducting Detectors Make a Difference? .....	22
<b>GEANT4 SIMULATIONS</b> .....	<b>23</b>
Overview of GEANT4 .....	23
The TES Model .....	25
Contributions to the Energy Spectrum .....	25
Am-241 .....	27
<i>Experimental vs. Simulation Data</i> .....	28
<i>Superconducting vs. HPGe Detectors</i> .....	29
<i>Different Absorber Sizes</i> .....	30
<i>Copper Ring vs. Copper Block</i> .....	31
Overview of RadSrc .....	32
Weapons Grade Uranium .....	33
Analyzing Plutonium .....	35
Spent Fuel Examples .....	37
<b>CONCLUSION</b> .....	<b>39</b>
<b>REFERENCES</b> .....	<b>41</b>
<b>APPENDIX A</b> .....	<b>43</b>
<b>APPENDIX B</b> .....	<b>45</b>

## INTRODUCTION

The safeguarding of nuclear materials is vital to the growth of the nuclear energy industry around the world. In the United States alone, the nuclear energy industry is expected to boom with Obama's administration favoring another \$37 billion in new loans to add to the \$18.5 billion accepted in 2005 [1]. It is the International Atomic Energy Agency's (IAEA) duty to verify that nuclear material around the world is accounted for at all stages of the fuel cycle. To successfully accomplish this task, the IAEA has established a series of different safeguarding techniques including methods for non-destructive analysis (NDA) and destructive analysis (DA). NDA is important in determining the characteristics of the material, such as enrichment and burnup, without the safety hazard of having to handle the radioactive substances.

Current NDA methods depend on efficient high-resolution detectors for either counting neutrons or detecting gamma rays. In the case of spent fuel analysis, NDA is used in conjunction with the declared operator values to verify the integrity of the material to ensure that it is not being diverted for other purposes, such as for the extraction of the fissile material. One of the widely used methods for NDA in spent fuel applications is gamma spectroscopy with high-purity germanium detectors (HPGe). These detectors are used to compare the isotopic ratios of fission products and retroactively determine the burnup. One of the biggest challenges in safeguarding is the direct detection of fissile material to determine isotopic composition in spent nuclear fuel. This is not easily achievable because the high Compton background originating from the fission products often obscures the gamma lines of the fissile material. Also the resolution is not high enough to make out low intensity peaks that are very close in energy. Very low temperature

ultra-high-energy resolution gamma-ray detectors such as superconducting TES cryogenic detectors may have the potential of addressing these concerns.

Superconducting detectors operating at around 0.1 K, offer over an order of magnitude improvement in the energy resolution over conventional HPGe detectors. The resolution leads to more discernable peaks in the dynamic range of the detector. These detectors are also quite small ( $\sim 1 \text{ mm}^3$ ) which causes the relatively low Compton background because the cross section of the higher energy gammas, that is responsible for the low-energy Compton background is small. The increase of the peak-to-background ratio at lower energies allows for easier detection of weak gamma rays. In order to understand and improve these superconducting detectors, GEANT4 is used to model the expected detector response. GEANT4 is a Monte Carlo simulation coded in C++ that allows the user to design a detector and pick the incident source. The program calculates all the energy deposited in the detector geometry, whether it be the full energy from the gamma ray or the partial energy after the gamma scatters within the shielding. In the case of complicated energy sources, RadSrc, a library used to calculate gamma ray distributions, is used to input the incident energies.

The thesis is broken down into four main sections. The first section discusses the duties of the IAEA and the current detection techniques used to identify spent fuel. This is followed by a description of the principles of operations of superconducting detectors and specifies what are the main advantages and limitations of these detectors. In order to discuss the detectors' potential use in identifying spent fuel, the third section focuses on current methods used to analyze spent fuel and how superconducting detectors can help solve a few unanswered questions. In the final section, the simulation model and results are discussed. The first series of simulations use Am-241 as the main gamma energy because its photopeak, at 60 keV, is within the dynamic

range of the detector. In these simulations the detector and shielding geometry are changed in order to analyze the effects on the spectrum. The next series of simulations use RadSrc to designate the incoming incident energy. Aged uranium and plutonium sources are used to analyze the detectors low energy response and discuss their applicability in directly identifying spent fuel. Finally the last set of simulations analyzes the response of spent fuel from pressurized water reactors (PWR), boiling water reactors (BWR) and Canada deuterium uranium reactors (CANDU).

## INTERNATIONAL NUCLEAR SECURITY

### The International Atomic Energy Agency

In 1945, the United States detonated two nuclear bombs over Japan, simultaneously ending World War Two (WWII) and unleashing the power of nuclear technology. Immediately after WWII, countries began a race against each other to develop a nuclear weapon of ever-increasing destructive power, believing that this was the type of warfare of the future. During this time period, the civilian applications to nuclear technology were also developed, leading to establishing nuclear energy as a viable and safe source of energy. The dilemma sprung when deciding how nuclear material and technology should be safeguarded to prevent the expansion of nuclear weapons but promote the use of nuclear energy.

The IAEA was created in 1957 after US President Eisenhower's "Atoms for Peace" address to the United Nations in 1953. The IAEA became powerful in 1968 when the Nuclear Non-Proliferation Treaty (NPT) came into effect essentially allowing the five countries that already possessed nuclear weapons to keep them, but preventing other nations to acquire

weapons. In return the non-weapons countries are given access to nuclear material and technology trade as long as they set up safeguard agreements with the IAEA, agreements that are backed by the threat of international sanctions. The IAEA today has 151 member states and it is in charge of assuring the world that nuclear technology is being used for the promotion of safe nuclear energy [2]. The Agency accomplishes its task by setting up a system of safeguards using a variety of detection techniques that allows them to monitor nuclear material at all stages of development, including the mining of raw material, the material enrichment process, the burning of nuclear material in power plants, the disposal of spent fuel and spent fuel reprocessing.

## The Threat of Nuclear Proliferation

The NPT was a great accomplishment when it passed in 1968, and the IAEA has been generally effective at being the “nuclear watchdog” of the United Nations. The IAEA has worked with countries to allow nuclear energy to be used without the fear of weapons. Nevertheless the IAEA is needed today more than ever to continually be at the forefront of detector technology in order to prevent the diversion of fissile material that could, for example, enable nuclear terrorism. Countries such as North Korea and Iran have been a focus point for the IAEA in recent years. In May 2009, North Korea bragged about successfully conducting its second nuclear test after asking the IAEA inspectors to leave the country years earlier [3]. In September 2009, it was revealed that Iran had enough nuclear fuel from its enrichment facilities to create a nuclear weapon [4]. A nuclear weapon, in an unstable country, in a region of conflict, is a recipe for disaster. The IAEA, in North Korea’s case, is essential in assuring the world that nuclear material is not being transferred into the country. In the case of Iran, the IAEA must properly safeguard the enrichment facilities to confirm that the nuclear fuel is used only for

peaceful purposes and inform the United Nations (as it already did) when it seems likely that the enriched uranium is not intended for use in nuclear energy. The IAEA must properly safeguard and account for all nuclear material. The task is not trivial given that there are 163 countries with safeguard agreements<sup>1</sup>, of which 72 have significant nuclear activity totaling 317,340 significant quantities of nuclear material<sup>2</sup> spread across 1131 facilities (see Appendix A) [5].

## Safeguarding Techniques

In order to safeguard nuclear material, the IAEA has implemented different safeguarding techniques to assure that the fissile material is accounted for at all stages of the fuel cycle, from the mining of raw uranium to the disposal of spent fuel. The main techniques include nuclear material accountancy, containment and surveillance, unattended and remote monitoring, and environmental sampling. Nuclear material accountancy entails counting items and using NDA to measure the attributes of the material and compare the results to operator declared values. The IAEA verifies the information declared by operators in search of gross or partial defects. Other techniques for partial defects entail weighing items to see if the core amount of mass is present. When looking for bias defects (small amount of change in the material over a large period of time) the best techniques involve applying chemical and physical processes to the material, a method known as destructive analysis (DA). Containment and surveillance techniques are used to maintain continuity of the knowledge learned through the various verification methods. After an inspector conducts a measurement they often seal the material container with an identifying

---

<sup>1</sup> The 163 countries include all countries with some sort of safeguard agreement in place, excluding the non-nuclear-weapon states signatory to the NPT that do not have any nuclear activity. Of the 163 nations, 84 have both comprehensive safeguard agreements and additional protocols in place; 70 only have comprehensive safeguards; 3 follow the INFCIRC/66/rev.2 and 5 have voluntary safeguard agreements [5].

<sup>2</sup> A significant quantity is defined by the IAEA as the approximate amount of nuclear material needed to create a nuclear explosive device. It is not the same as critical mass because it takes into account the amount of material lost in the conversion and manufacturing stages [5].



tag. Optical surveillance can then be used to account for the integrity of the container. This method saves time by allowing the inspector to not have to redo measurements in certain situations, such as verifying the integrity of spent fuel in storage ponds. Unattended and remote monitoring techniques combine some of the containment and surveillance methods with NDA to safeguard areas that operate over extended periods of time without inspector access. In these cases, the data are collected 24 hours a day, 7 days a week by employing radiation detectors to detect the flow of nuclear material or through security cameras. The most important aspect of remote monitoring is data security, and the inspectors need to be able to have a constant flow of untainted information. The final technique employed by the IAEA is environmental sampling, which was initially implemented to allow inspectors to swipe samples in enrichment plants. The technique is now being extended to different nuclear facilities and involves collecting environmental samples at or near a nuclear site. The sample is then sent to a laboratory to be analyzed using ultrasensitive techniques in the hopes of revealing information about present or past activities in the area. [6]

## Non-Destructive Analysis

Non-destructive analysis allows inspectors to collect data without having to destroy or change the material. This is less time-consuming than destructive analysis, and is useful for safeguarding nuclear facilities or identifying unknown nuclear material in situations where handling the material can pose a hazard to the inspector. The two main NDA techniques are gamma ray spectrometry and neutron counting. Gamma ray spectrometry is a form of NDA used to detect the energy and intensity of the gamma rays emitted by the material. The gamma ray energy is used to determine the source material, and the gamma ray intensity is used to determine

the material abundance in the sample. The data collected are then used to compare the values to the declared operator values to look for inconsistencies in the numbers [7].

The most common gamma ray detector types used by the IAEA are scintillators (NaI) and semiconductors (HPGe, CdZnTe). Sodium Iodide (NaI) detectors are useful as a first line of defense because of the high efficiency and portability of the device. These types of detectors can be used to detect the presence of spent fuel, but due to their low energy resolution they are not useful for characterizing low energy gammas or the isotopic composition of spent fuel. Semiconductor detectors offer a higher energy resolution than scintillators. Cadmium Zinc Telluride (CdZnTe or CZT) detectors are portable, small, do not require cooling, and have a high intrinsic energy efficiency. High-purity Germanium (HPGe) detectors are the detectors with the highest energy resolution that are available in the market. They can be used to identify complex spectra and isotopic compositions. However, they must be cooled with liquid nitrogen to reduce thermal noise [6]. A comparison of the spectra produced by these three detector types is shown

**Table 1:** Gamma-ray spectrometers currently used by the IAEA to safeguard nuclear material.

Code	Detector Type	Instrument	Primary Application
HM-5	NaI or CdZnTe	Hand-held Assay Probe	Qualitative determination of the presence of U, Pu and other isotopes
IMCN, IMCC, IMCG	NaI, CdZnTe or HPGe	I-2000 Multichannel Analyzer used with a gamma spectrometer	Verification of U enrichment, spent fuel and Pu composition
MMCN, MMCC, MMCG	NaI, CdZnTe or HPGe	Miniature Multichannel Analyzer used with a gamma spectrometer	Verification of U enrichment and spent fuel

*Source: IAEA, "Safeguards Techniques and Equipment," International Nuclear Verification Series, Vienna, Austria, No. 1 (Revised), IAEA (2003).*

in figure 1. Table 1 depicts the main gamma ray detectors used by the IAEA for NDA and their primary safeguarding applications.

The other main form of NDA is neutron counting; by measuring the neutron intensity the inspector can deduce how much material is present. Neutrons can penetrate deeper into matter than gamma rays, which make them easier to measure. However, the neutron energy cannot be used to identify the material. There are two main methods to count neutrons: passive and active coincidence counters. Neutrons are primarily emitted through spontaneous fission and induced fission in groups of two or more per fission event. Single neutrons are also emitted through alpha particle interactions. When measuring the intensity of neutrons, the significant neutrons are the

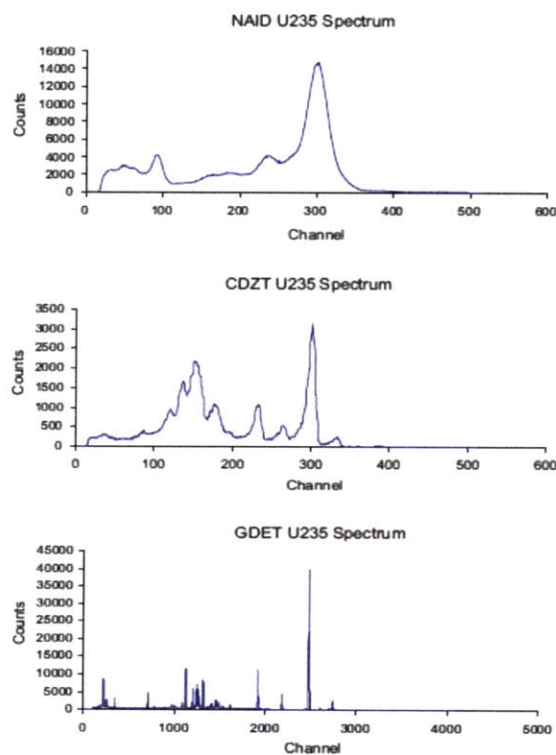


**Figure 1:** Comparison of the gamma ray spectrum for U-235 using a sodium iodine (NaI), cadmium zinc tellurium (CdZnTe) and high-purity germanium (HPGe) detector. These are the three main instruments used by the IAEA to safeguard nuclear material.

*Source: IAEA, "Safeguards Techniques and Equipment," International Nuclear Verification Series, Vienna, Austria, No. 1 (Revised), IAEA (2003).*

ones that are produced via fission. In order to reduce the background the detector systems therefore measure multiple neutrons signatures by time related coincidences. The mass of Pu can be determined by knowing the isotopic abundance of Pu-239 (commonly determined using gamma-ray spectrometry) and by measuring the neutrons emitted by spontaneous fission. This is an example of a passive counter because the source undergoes sufficient spontaneous fission to be significant. In the case of isotopes that do not spontaneously fission, such as U-235, an external neutron source is used to induce fission [6].

## Limitations of Current Detector Technologies

The choice of detectors is largely dependent on the primary application it is intended for. The two important properties that affect detection are efficiency (intrinsic and geometric) and energy resolution. The intrinsic efficiency depends on the detector materials, while the geometric efficiency depends on the size and layout of the detector. In a simplified layout having a point source at a distance  $r$  from the detector with area  $A$ , the geometric efficiency ( $\epsilon_{\text{geometric}}$ ) is defined as

$$\epsilon_{\text{geometric}} = \frac{A}{r^2} \quad [8]. \quad (1)$$

The size of the detector and the location of the source are important for determining efficiency. Current detector methods are fairly efficient; however, they sometimes lack the energy resolution needed to identify low energy gamma rays because of the high Compton background and line overlap. The size of the detector is often increased in order to increase efficiency; however this increases the cross section for higher energy gammas that are responsible for the low energy Compton background. In the case of nuclear safeguards, fissile material is often masked by the

high Compton background because there are several low energy identifying gamma rays in plutonium.

## SUPERCONDUCTING DETECTORS

Superconducting detectors operated at temperatures around 0.1 K (figure 2) use the reduction of thermal noise at very low temperatures to offer an order of magnitude increase in resolution over conventional HPGe detectors. The increase in resolution is particularly useful at

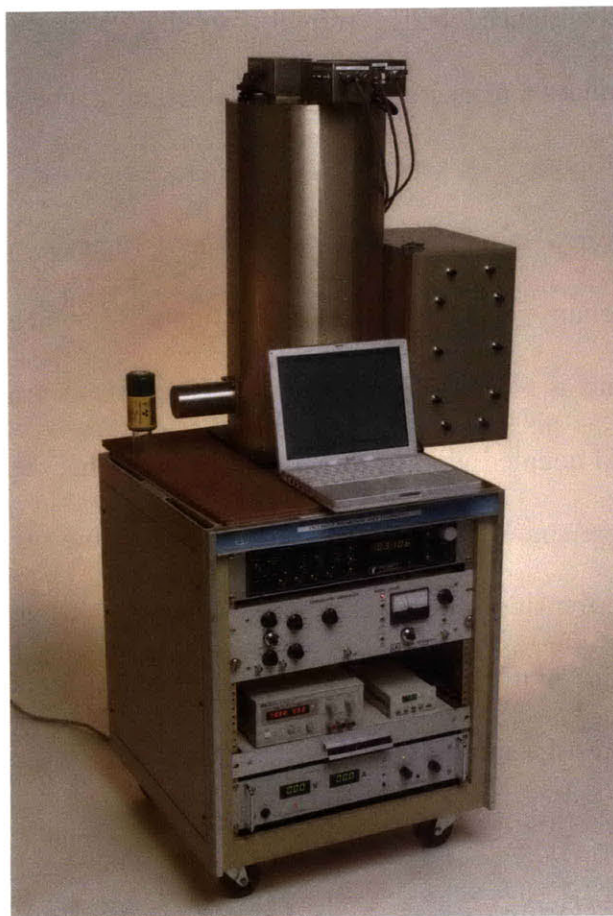


**Figure 2:** Superconducting gamma ray spectrometer with readout electronics.

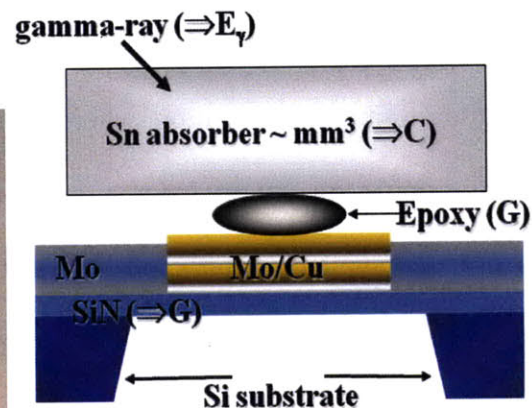


**Figure 3 (left):** Schematic representation of the detector setup using a Mo/Cu TES and a Sn absorber.

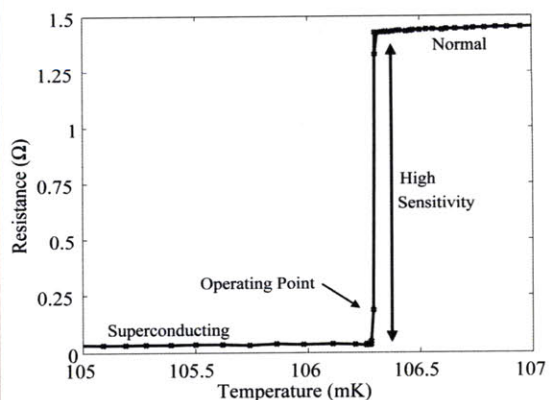


**Figure 4 (right):** The transition between the normal and superconducting state for a Mo/Cu TES absorber.

identifying lower energy gamma rays with similar energies. Since the volume of the detector is quite small ( $\sim 1 \text{ mm}^3$ ), the cross section for high-energy gammas is low and therefore the Compton background is reduced. The increase of the peak-to-Compton ratio allows the detectors to be ultra-high-energy resolution and have a series of useful applications in nuclear safeguards.

## Detector Components

Superconducting gamma-ray detectors are composed of a bulk absorber with heat capacity  $C$  and a superconducting sensor that is weakly coupled to a cold bath through a silicon nitride membrane with thermal conductance  $G$ . The sensor is operated at the temperature of the superconducting-to-normal transition where its resistance changes rapidly, so that even the absorption of a single low-energy gamma ray produces a measurable change in resistance. These types of sensors are typically referred to as transition-edge sensors (TESs). The detectors that are currently being tested at Lawrence Livermore National Laboratory (LLNL) have a  $\sim 2 \times 2 \times 0.25 \text{ mm}^3$  tin absorber and a molybdenum-copper (Mo-Cu) TES (figure 3), which transitions from its normal to superconducting state at  $\sim 0.1 \text{ K}$  (figure 4). The two elements are strongly coupled to each other through epoxy, and coupled weakly to the cold bath, so that the TES can be heated briefly above the cold bath temperature upon gamma-absorption in the tin. Superconducting detectors exploit the sharp phase transition of the TES because a small change in the temperature translates into a non-trivial change in the resistance. Therefore when a gamma ray is incident upon the absorber the TES measures the intensity of the ray as a change in the resistance. Since the TES resistance change is very low ( $\ll 1\Omega$ ), a superconducting quantum interference device (SQUID) is used as a preamplifier.

One of the distinguishing characteristics of superconducting detectors is that they operate at extremely low temperatures to attain extremely high-energy resolution. In order to achieve these low temperatures the TES is held at the end of a cold finger connected to a multi-stage cryostat, with a nested design composed of different temperature levels. The first two levels pre-cool the detector using liquid nitrogen to get to 77 K and liquid helium to get to 4.2 K. From here, the detector is cooled to its operating temperature of  $\sim 0.1$  K using a two stage adiabatic demagnetization refrigerator (ADR). The adiabatic demagnetization process involves aligning the spins of two different paramagnetic salts in a large superconducting electromagnet, while carrying the heat of magnetization to the helium bath through a closed heat switch. After the paramagnets are equilibrated at 4.2 K, the heat switch is opened and, the magnetic field is lowered slowly, thereby allowing the spins of the paramagnets to randomize and take in energy in the form of heat. The first paramagnetic salt used at LLNL in the initial stage, to cool to  $\sim 1$  K, is a gadolinium gallium garnet ( $\text{Gd}_3\text{Ga}_5\text{O}_{12}$ ). The second salt that cools to  $\sim 0.06$  K is iron ammonium sulfate ( $\text{Fe}(\text{NH}_4)(\text{SO}_4)_2$ ), usually referred to by its antiquated name ferric ammonium alum (FAA) [9]. Once the cooling is complete the detector is able to operate for 8 to 20 hours depending on the operating conditions.

## Principles of Operation

The absorber and the TES are chosen in order to optimize the energy resolution ( $\Delta E_{FWHM}$ ), which in the simplest case [10] has a value of

$$\Delta E_{FWHM} \approx 2.355\sqrt{k_B T^2 C}, \quad (2)$$

where  $k_B$  is the Boltzmann constant and  $T$  is the temperature. The energy resolution is mostly limited by thermodynamic fluctuations between the sensor and the cold bath, also known as phonon noise. One can illustrate the origin of equation (2) by assuming that a phonon at energy  $T$  carries an average energy of  $k_B T$ , and the absorber's total energy is  $CT$ . Then the total number of phonon modes is  $CT/k_B T$ , or simply  $C/k_B$ . The phonons will fluctuate, according to Poisson statistics, by  $\sqrt{C/k_B}$ . This fluctuation in the phonon number is then multiplied by the energy per phonon,  $k_B T$ , in order to calculate the energy root mean square (rms) fluctuation of  $\sqrt{k_B T^2 C}$  [9]. A more complete derivation of the energy resolution takes into account the Johnson noise in the TES, the effects of temperature gradients in the thermal link and the optimization of the signal shaping filters. The more extensive derivation proves that equation 2 is correct for weakly coupled systems and strong coupling between absorber and TES at a certain set temperature.

From equation 2, high-energy resolution, i.e. lower  $\Delta E_{FWHM}$ , is achieved by lowering the temperature ( $T$ ) and lowering the heat capacity ( $C$ ). The operating temperature is set by the TES's normal-to-superconducting transition temperature, and by the practicality of achieving the low temperature desired. The optimal temperature of 0.1 K can be achieved with modern ADR technology. The heat capacity  $C$  is set by the absorber material and its volume. The absorber volume is therefore kept small, and absorber materials are preferred that do not have an electronic contribution to the specific heat, such as superconductors, insulators or semi-metals. In order to achieve an energy resolution of 100 eV with Sn the necessary absorber volume is  $\sim 1 \text{ mm}^3$ . Heat capacity also sets the count rate capabilities of the detector because the thermal relaxation time must be taken into account. The relaxation time ( $\tau$ ) is the time it takes the detector to return to the cold bath temperature after being hit by a gamma ray, and is given by



$$\tau = \frac{C}{G} \quad [9]. \quad (3)$$

For typical gamma ray detectors, this relaxation time is on the order of ~ms, which sets the maximum count rate of a superconducting TES detector to a few tens of counts/s per detector pixel.

## Detector Tradeoffs

Superconducting detectors offer a very high-energy resolution. However, they do have a slow count rate, they require long cooling periods and they have a limited dynamic range. The detector itself is quite small and the count rates are slow (50-100 c/s) compared to a typical HPGe detector (~5000 c/s). The low count rate means longer detection periods, in order to collect sufficient counts to make a significant measurement. An instrument used in the field will require a quicker count rate, and therefore new designs with arrays of TESs are being developed to increase the collecting area and total count rate [11]. Another important aspect of instruments used in the field is portability. Superconducting detectors require extensive cooling that takes a fair amount of time and resources to cool. Research is being conducted to create new cryogenic coolers that are smaller and more efficient, although superconducting technology will likely never be used in hand-held instruments [12]. Finally, superconducting detectors have a limited dynamic range due to the intrinsic nature of the device, which can be driven off the normal-to-superconducting transition if the energy of the incident gamma ray is too high. The detector applications are therefore limited to low-energy gamma rays below ~200 keV. This is however, usually less of a restriction since most of the line overlap problems in NDA occur in the low-energy range.

## Applications of Superconducting Detectors

Superconducting detectors offer an order of magnitude improvement over conventional high-purity germanium (HPGe) detectors, and may therefore have a potential application in the non-proliferation safeguarding work done by the IAEA. These detectors have potential applications in all stages of the fuel cycle. When dealing with uranium mining, the ultra-high energy resolution detectors can determine the ratio between uranium and its daughter products such as Ra-226 in the tailings from mining operations. This allows inspectors to detect illegal uranium mining. Superconducting detectors can precisely determine the enrichment of uranium by examining the thorium lines at 92 keV instead of the traditional 186 keV U-235 line that NaI detectors identify [13]. This thesis will focus on the case of spent fuel where the gamma rays emitted are often masked by the high Compton background, and will examine if TES detectors offer improved analytical capabilities.

### SPENT FUEL

There are several different kinds of detectors used by the IAEA to determine in a non-destructive manner the amount of fissile material present in irradiated nuclear fuel. Indirect signatures based off of the strong gamma or neutron emitting fission products, such as Cs-137 and Cm-242, are used to determine burnup and to calculate an estimate of the plutonium buildup. These numbers are compared to the declared operator value to verify compliance or detect any inconsistencies. In the case of fuel assemblies, each unit is stamped with an identification number that is used to track the material throughout its lifetime. Besides burnup, it is also essential to know the fissile content of material. Fresh fuel can be characterized using detection

techniques that measure directly the amount of uranium and plutonium in the material. However, once the fuel is irradiated, the signature lines used to detect uranium and plutonium are masked by the strong radiation emitted from the fission products, which build up throughout the reactor cycle, making the U and Pu much harder to detect [14]. Active interrogation techniques also exist, however they will not be discussed here.

## Burnup Calculations

If the spent fuel is in a storage pond, then Cerenkov light can be used to determine the presence and burnup of irradiated fuel. Beta particles, gammas and neutrons can emit Cerenkov radiation, which occurs when a charged particle passes through a medium, such as water, in which its velocity exceeds the phase velocity of light. The absolute Cerenkov light level along with the decay time can be related back to burnup. Gamma ray and neutron activity counts do not require the spent fuel to be submerged in water [14]. In the case of gamma ray activity, the total buildup activity of a single fission product can serve to identify burnup if:

1. The uranium and plutonium yields are equal.
2. The neutron cross section of the fission product is small to ensure that secondary neutron capture reactions are not factored into the fission product activity.
3. The half-life of the fission product is significantly longer than the irradiation time to accurately account for the number of fissions.
4. The gamma-ray energy is relatively high to be able to escape from the fuel pin [14].

Once these conditions are satisfied, the measured fission product gamma ray activity ( $I$ ) can be used to solve for the number of fission product nuclei ( $N$ ) formed during the irradiation period:

$$N = \frac{Ie^{\lambda T}}{\epsilon k S \lambda} , \quad (4)$$

where  $\varepsilon$  is the absolute detector efficiency,  $k$  is the branching ratio,  $S$  is the attenuation correction,  $\lambda$  is the decay rate and  $T$  is the cooling time [14]. Using Equation 4 the percent fuel burnup ( $B$ ) is

$$B = 100 \times \frac{(N/Y)}{U}, \quad (5)$$

where  $Y$  is the fission product yield and  $U$  is the number of initial uranium atoms [14]. Due to Cesium-137's high gamma energy and long half-life, it is commonly used as the fission product gamma ray activity indicator for fuel burnup. The measured burnup is then used to estimate the amount of fissile material, which is then compared to the value declared by the reactor operator.

The burnup of irradiated fuel can also be determined using fission product ratios. The most common isotopic ratios used are Cs-134/Cs-137 and Eu-154/Cs-137. Cs-134 requires two neutron interactions making the concentration of Cs-134 proportional to the square of the integrated flux. Cs-137 is directly proportional to the flux, therefore the ratio is approximately proportional to the burnup [14]. Things to consider when using isotopic ratios are that the numbers must be corrected for decay time and the detector efficiency must be taken into account.

Another technique used to indirectly analyze spent fuel is by calculating the total neutron output of the material, which can be measured directly after fuel discharge. This is an advantage over gamma ray spectrometry because immediately after the discharge, the gamma ray signal is dominated by the decay of short-lived isotopes. There are five main neutron sources in spent fuel; the two dominant neutron-emitting isotopes are Cm-244 and Cm-242. These isotopes have a short half-life therefore it is essential to know the cooling time, which are declared by the operator and verified by measuring the total gamma ray activity [14].

## Detector Technology

To complete indirect measurements of irradiated fuel there are several different detection techniques in use. Cerenkov radiation is the easiest and fastest radiation measurement that uses a simple hand held detector composed of an image amplifier and photomultiplier tube used to measure the intensity of the light passing through. When a fuel assembly is submerged in water, ion chambers, scintillators and thermoluminescent dosimeters are used to measure the total gamma-ray activity. For more precise gamma ray measurements, HPGe detectors with a long, air filled collimators are used for identifying fuel assemblies in storage ponds. Gamma rays do not penetrate as deep as neutrons do, but their attenuation in water is not as severe. Neutron detectors must be close to the fuel assembly, therefore require the material to be partially lifted out of the storage racks. Fork detectors are the most commonly used detectors for fuel assemblies. The detector consists of two sets of ion chambers and fission chambers to simultaneously measure both sides of the assembly. The ion chambers measure the total gamma ray output, while the fission chambers operating in pulse mode measure the neutron output [14].

## The Spent Fuel Problem

The detector technology currently available does not allow for the direct measurement of gamma ray and neutron signatures of uranium and plutonium isotopes. There are two possible approaches to determine the concentration of fissile material. The first one uses calculated or empirically determined correlations that relate burnup to residual U-235 and plutonium content. Due to time and manpower constraints, it is common to measure the burnup levels of each assembly at only one position along the length to verify the operator declared value. The

concentration of fissile isotopes is then calculated using complex simulations such as CINDER. The results of the calculations lead to a plot of the concentration of fissile isotopes as a function of burnup. These calculations are difficult to accurately perform due to the many different measurement values and reactor core parameters involved. The second approach directly measures the fissile content of spent fuel using active neutron interrogation. However, these devices are not common because they require an accelerator or neutron generator to induce fissions [14].

## How can Superconducting Detectors Make a Difference?

Superconducting detectors have the potential to measure the low-energy plutonium and uranium signature gamma rays, even in the presence of a sizeable Compton background, because their small size reduces the level of the Compton background, and their high-energy resolution makes the lines stand out above this background more clearly. A direct measurement might allow inspectors to determine, using NDA, the fissile content of the spent fuel that can be used to identify the material. Other applications for superconducting detectors in the context of spent fuel assay might include measuring:

- The uranium isotope ratios to indicate the enrichment activity.
- The minor isotope ratios to learn about the enrichment processes and feed materials.
- The presence of certain fission products that indicate the processing of spent fuel.
- The Pu-240/Pu-239 ratio to indicate fuel burnup.
- The radioactive parent-daughter ratios (Am-241/Pu-241) as a way to indicate the time since the last chemical separation [15].

# GEANT4 SIMULATIONS

## Overview of GEANT4

A gamma-ray interacting in matter has a number of different possibilities as to how it deposits its energy, making its energy deposition in a superconducting detector a good candidate for Monte Carlo simulations. Monte Carlo is a class of computational algorithms that rely on the probability of an event to occur to randomly calculate the outcome. GEANT4 is a Monte Carlo modeling package coded in C++ used to track the interaction of particles through matter. The user of GEANT4 decides on a stepsize, so every time the particle advances one step, the program semi-randomly evaluates what the next move of the particle will be. The decision is semi-random, because it is based off of a physics list that sets the likelihood of different interactions occurring [16]. If the simulation is run with 10 events, chances are that only the most common interactions will occur. If the simulation is run with millions of events, then the probability that all interactions will be visible is quite high. Therefore, for favorable results the stepsize should be less than the thickness of the material the particle is going through, and the number of events processed should be large. In our simulations we used a stepsize of 0.01 mm with a minimum of  $10^7$  events per configuration.

GEANT4 allows the user to add geometries into any configuration and then decide which part will act as the sensitive detector. The energy spectrum is taken in the reference frame of the sensitive detector, and only the energy deposited in the detector is recorded. For example, if a photon misses the detector, hits the background material and scatters back into the detector, the energy lost in the scattering event is not recorded, but the energy deposited in the detector when it scatters back is. In our simulation the sensitive detector is composed of a  $1 \text{ mm}^3$  piece of tin, which serves as the absorber of the TES.

The physics list included in GEANT4 allows the user to choose what particle type to use as the incident source. The program also gives the user control as to how the source is going to hit the geometry. The source can be modeled as a point source shooting randomly in all directions, or as a linear source shooting in a random x-y direction. In our simulations the particle gun is a point source shooting in the forward and the backward direction with an angle span of  $\pm 32.74^\circ$ . This is done because the source is encapsulated in a steel cylinder with a small tunnel for the gamma-rays to be guided out, as seen in figure 5. If the source was modeled as a true point source, too much of the events stayed within the cylinder and never reached the detector, leading to a poor spectrum at a high computational cost. Therefore the gun was

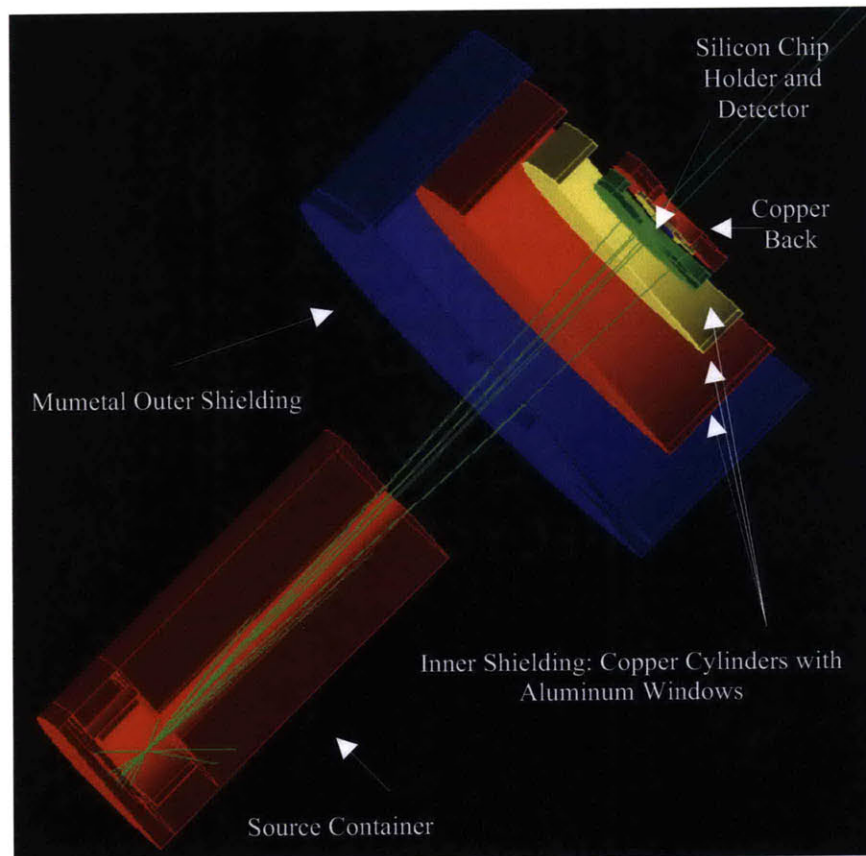


**Figure 5** GEANT4 model of a TES superconducting detector and the steel container used to encapsulate the model source.



restricted to include just the scattered photons from the steel container that actually reached the detector.

## The TES Model

The model of our superconducting detector (figure 5) is composed of a tin absorber of about  $1 \text{ mm}^3$  surrounded by a silicon chip holder and a copper heat sink behind the absorber. Four layers of shielding surround the absorber representing the different temperature stages. The outer layer is made out of mumetal, which is mostly nickel, and the three inner layers are copper cylinders with a  $25\mu\text{m}$  thick aluminum window used for thermal shielding of the detector.

## Contributions to the Energy Spectrum

There are different contributions to the response function in superconducting TES gamma detectors. The photopeak occurs when the gamma ray photon is completely absorbed by the material. In addition to the main peak, there are several other features in the response function that determine the detector's sensitivity. Figure 6 depicts the different sources of the background spectrum that lead to less than the full energy being deposited in the detector. Compton scattering occurs when an incident photon ( $h\nu$ ) hits an electron causing the creation of a scattered lower energy photon ( $h\nu'$ ) and a recoil electron. The energy of the scattered photon depends on the scattering angle ( $\theta$ ) and is given by

$$h\nu' = \frac{h\nu}{1 + \left(\frac{h\nu}{m_0c^2}\right)(1 - \cos\theta)}, \quad (6)$$

where  $m_0c^2$  (511 keV) is the rest mass energy of the electron [17]. If the scattered photon leaves the material, only part of the energy is deposited in the absorber, hence the origin of the

Compton continuum. The Compton continuum is broad because the energy lost ranges from the lowest energy loss ( $\theta=180^\circ$ ) to the greatest energy loss ( $\theta=0^\circ$ ). If the photon is not incident on the absorber but instead Compton scatters in the material behind the absorber and the scattered photon is subsequently absorbed in the detector, a backscatter peak is created. The energy ranges from the lowest energy at  $\theta=180^\circ$  to the greatest possible scatter that still hits the absorber. If the photon Compton scatters in the material in front of the absorber it has a similar effect except that it scatters from the shielding. Compton scattering also creates a recoil electron that interacts with the material. When an electron is set loose in the absorber, it loses its energy by hitting other electrons, which leads to a cascade of electrons interacting with each other. This only becomes significant from our standpoint when the electron leaves the absorber therefore not all of the energy is deposited leading to extra scattering events.

Some other features of the energy spectrum are the escape and fluorescence peaks. The escape peaks occur when a photon hits the absorber and ejects an electron from the inner atomic

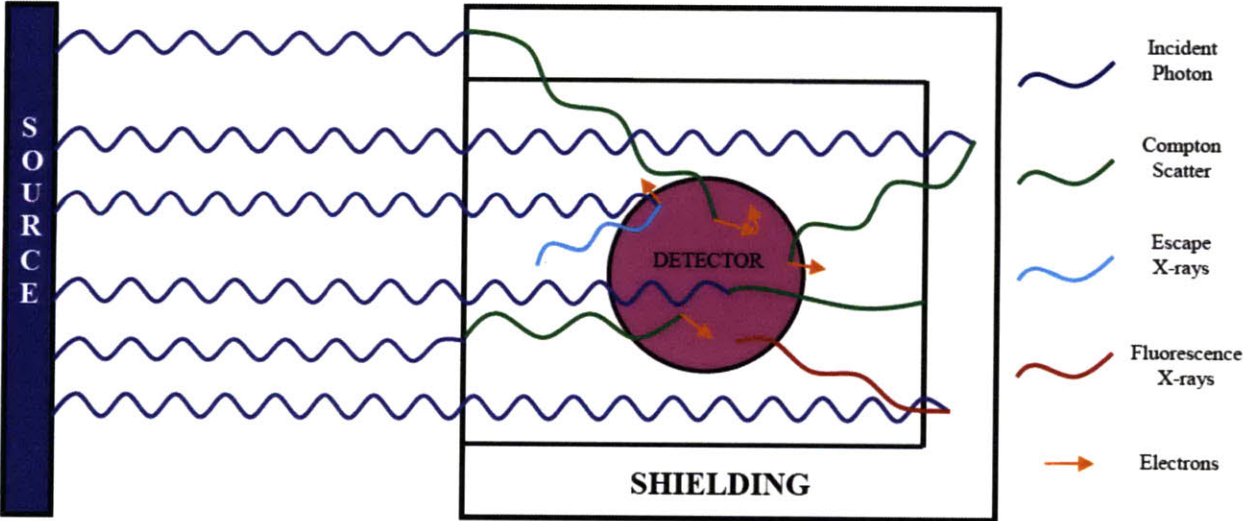


**Figure 6** Possible interactions of a gamma source incident on an absorber neglecting pair production.

shell (usually the K or L shell) leaving an electron hole. The energy needed to eject the electron depends on the specific binding energy associated with the material in that specific orbital. The electron hole leaves the atom unstable and causes an outer orbital electron to fall down to that energy, emitting an x-ray. If this fluorescence x-ray escapes from the absorber, an escape peak occurs in the spectrum, and its energy can be calculated by subtracting the known x-ray energy from the photopeak. Fluorescence peaks are created the same way as escape peaks, except that the incident photon hits the material surrounding the detector instead of the absorber itself. If the emitted x-ray is subsequently captured by the absorber and deposits its full energy in it, it creates a peak in the energy spectrum at the characteristic energy of the x-ray emitted. Another common mechanism of gamma interaction is pair production, which can be neglected here because our sources do not produce lines above 1022 keV.

## Am-241

Americium-241 has a prominent gamma ray at an energy of 60 keV, which falls into the detector's dynamic range. Several simulations were performed with this gamma energy to understand the low energy capabilities and qualities of the simulations. The different contributions to the response function are clearly labeled in each of the figures. Some of the common features of Am-241 include the photopeak at 60 keV, Compton scattering and a few other peaks dependent on the detector itself. In the case of superconducting detectors, these include the tin escape peaks:  $K_{\alpha 1}$  at 25.271 keV,  $K_{\alpha 2}$  at 25.044 keV and  $K_{\beta}$  at 28.486 keV. The less intense L escape peaks are also visible. The L x-rays have lower energies, which range from 3.443 to 3.904 keV.

## Experimental vs. Simulation Data

In order to analyze how closely the GEANT4 simulation matches the actual experimental data from superconducting detectors, figure 7 plots the two spectra together. The features of the spectrum match quite closely to the experimental data. Features such as the tin escape peaks, and the Compton scattering in the detector match very closely. However the backscatter peak at around 50 keV is greater for the experimental data and the 8 keV copper fluorescence is only present in the simulation results. The discrepancies between the spectra are due to the simplification of the geometry used in the simulations causing an overall smaller backscatter peak. For example, the copper fluorescence is most likely being reabsorbed by the 5  $\mu\text{m}$  gold

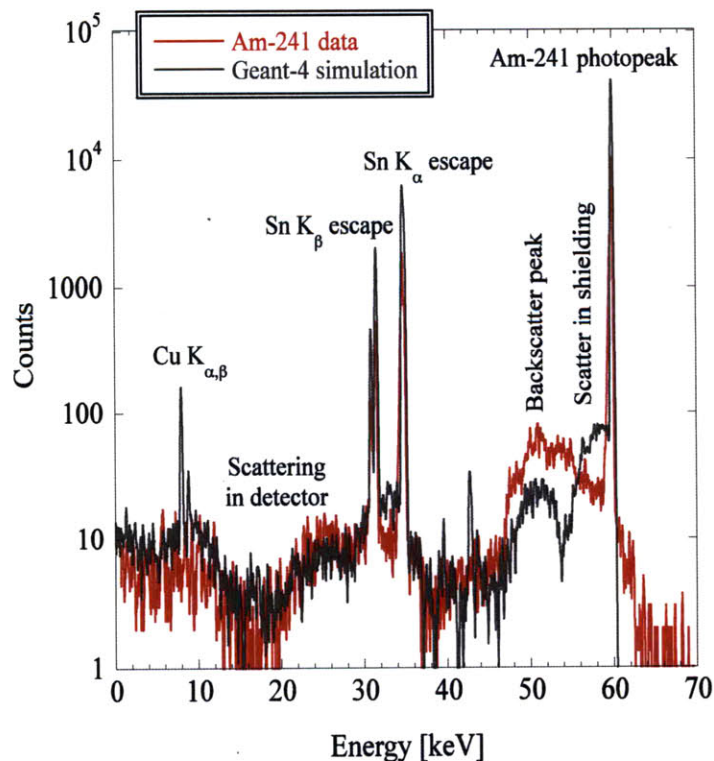


**Figure 7:** Comparison of the simulation including the copper back and the aluminum/nickel shielding to the experimental data for a 60 keV (Am-241) source.

coating on the copper, which is not modeled in the simulation.

### Superconducting vs. HPGe Detectors

The main advantage to TES detectors is the increase in energy resolution and the high peak-to-background ratio. Figure 8 plots the energy spectrum for a conventional HPGe detector against the simulation of a superconducting detector. The HPGe detector is much more efficient therefore the counts of the germanium detector were scaled down to be able to accurately compare the photopeaks. The full-width half-max (FWHM) of the photopeak for the HPGe spectrum is 1.15 keV. The resolving power (R) can be determined assuming that

$$R = \frac{FWHM}{H} \quad [17], \quad (6)$$

where H is the height of the peak minus the height of the background. The HPGe resolution is  $\sim 6.3 \times 10^{-6}$ , while the resolution of the TES detector is  $\sim 8.9 \times 10^{-7}$ . The peak-to-background

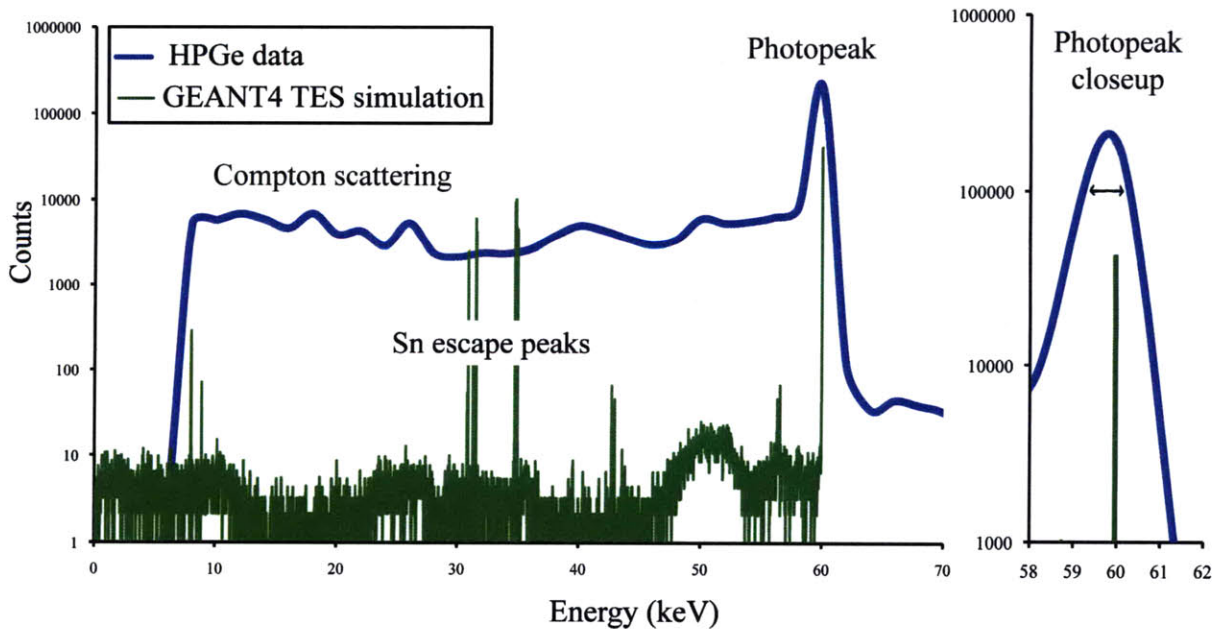


**Figure 8:** Comparison of the GEANT4 simulations results for Am-241 with data taken by an HPGe detector.

ratio is  $\sim 64$  for the HPGe detector data, which is significantly lower than the  $\sim 1,500$  for the superconducting detector. The ultra-high-energy resolution of the TES detector along with the high peak-to-Compton ratio produces a very powerful tool for gamma spectroscopy. Different gammas that have very similar energy can be identified from each other because of the discrete peaks. Also as seen in the simulation spectrum, the background is not very high, and is therefore not hiding any of the peaks. Superconducting detectors offer a much clearer spectrum than the HPGe detector. Nevertheless, an HPGe detector has a higher count-rate and requires less cooling steps. For a field experiment, the HPGe detector is preferred. For a detailed material composition analysis, a superconducting detector is preferred.

## Different Absorber Sizes

The size of the tin absorber is an important factor in determining the response of the spectrum. The simulation models were ran with a copper block in the back, keeping the volume of the tin absorber at about  $1 \text{ mm}^3$  but changing the dimensions. As seen in figure 9, the thinner the absorber (0.25 mm), the higher the photopeak because it increases the surface area of interaction. The absorption length at 60 keV is smaller than the 0.25 mm thickness, and therefore the increase in surface area increases the number of interactions. The photopeak will continue increasing for thinner absorbers as long as the thickness does not go below the absorption length. The backscatter is also slightly greater for the thinner absorbers, but if you compare the ratio of the photopeak to the backscatter peak, the ratio is larger for the thinnest absorber. The ratios range from  $\sim 420$  for the thickest absorber and  $\sim 1,470$  for the thinnest one. The larger the ratio, the easier it is to determine the peaks from the background and to identify the source materials.

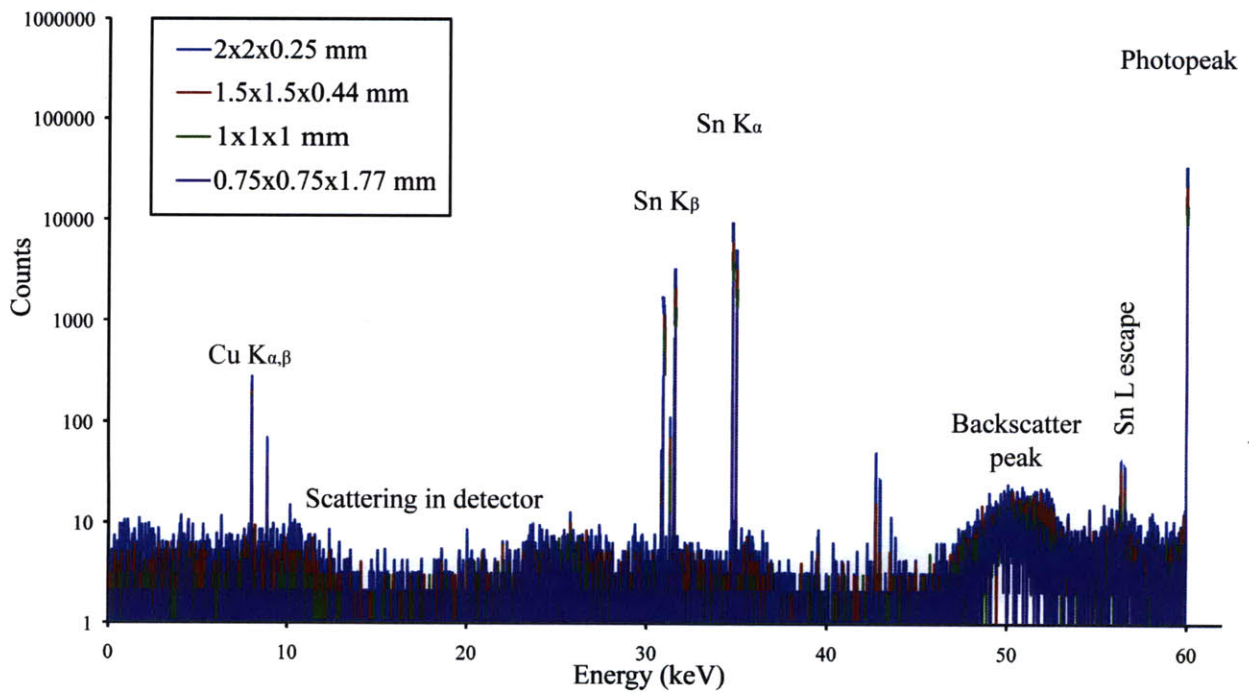


**Figure 9:** Simulation of a 60 keV gamma source incident on a 1 mm<sup>3</sup> tin detector of different dimensions.

### Copper Ring vs. Copper Block

The response function is sensitive to the various different detector components, and the spectrum can drastically change when the geometry of one of the object changes. This is apparent back in figure 7, when the experimental data does not perfectly fit the simulation data. There is some difference in the simulation geometry that changes the scattering within the detector. The energy spectrum seen in figure 10 compares the results from running the simulation using a copper block on the back and then a copper ring as the back. The copper block spectrum has a slightly higher backscatter peak due to the fact that less gamma rays were able to scatter away from the copper block into the detector. The simulation only measures the gammas that deposit their energy in the sensitive tin absorber. Another interesting difference

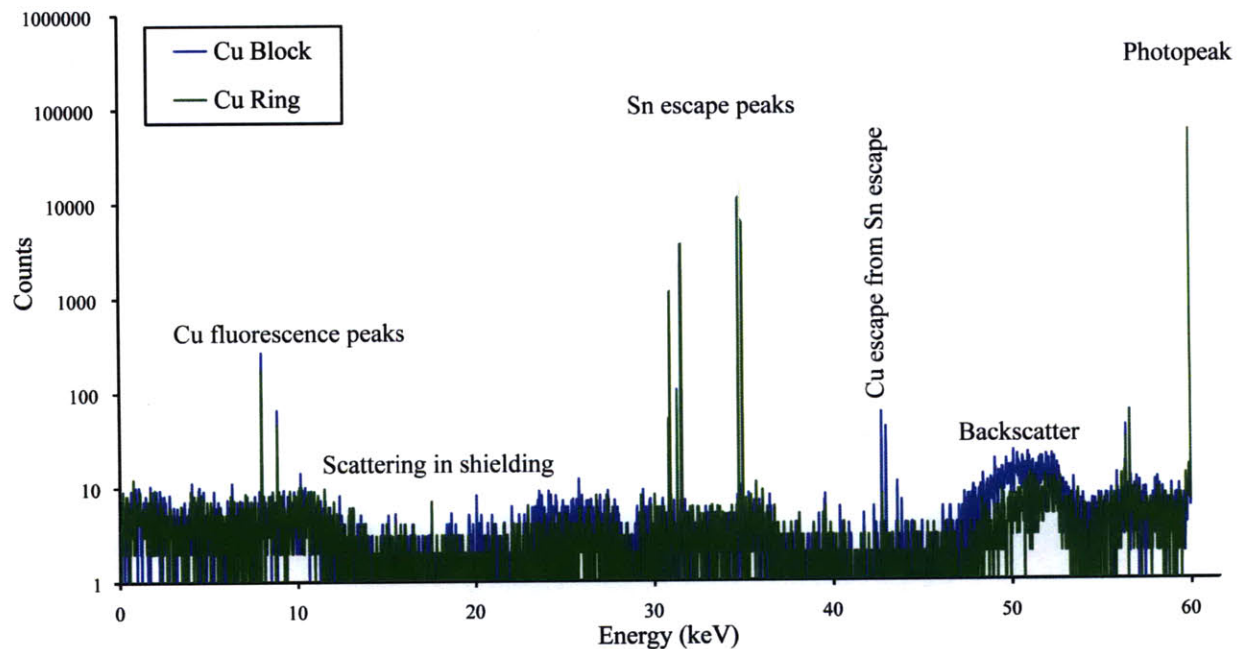


**Figure 10:** Comparison for a Am-241 (60 keV) gamma source when the copper block behind the detector is substituted for a copper ring.

between both simulations is the decrease in the copper escapes with the ring geometry due to the fact that there is less copper for the gammas to interact with.

## Overview of RadSrc

RadSrc, written in C++, is a computational program used to calculate the gamma ray energy distribution of a radioactive source. The user inputs a specific set of isotopes, and Radsrc ages the material to a specified number of years, calculates the concentrations of the decay products and outputs a complete energy spectrum. The RadSrc library (libradsrc) has four main components: the isotope database, decay product calculations, photon intensity calculations and interfacing routines. The program combines the radioisotope data, x-ray and gamma ray line catalogues, to calculate the photon emission of an aged sample [18]. Radsrc outputs files with the new material composition and the intensity of different gamma emissions include the parent



nuclide of each emission and the decay chain it is derived from. One of the most useful applications is the ability to interface RadSrc with several Monte Carlo transport codes including MCNP, COG and GEANT4. For the next series of simulations RadSrc is integrated into the GEANT4 simulations to analyze the potential spectrum produced by these detectors and determine their feasibility for spent fuel analysis.

### Weapons Grade Uranium

The direct identification of fissile content is important in spent fuel analysis. U-235 and Pu-239 are two important fissile materials that can be used to create weapons. The following two simulations analyze weapons grade uranium and plutonium. The first input (see Appendix B) into the TES simulation using Radsrc is of weapons grade uranium that has been aged 30 years. The point of the simulation is to analyze the main uranium emission lines to determine the

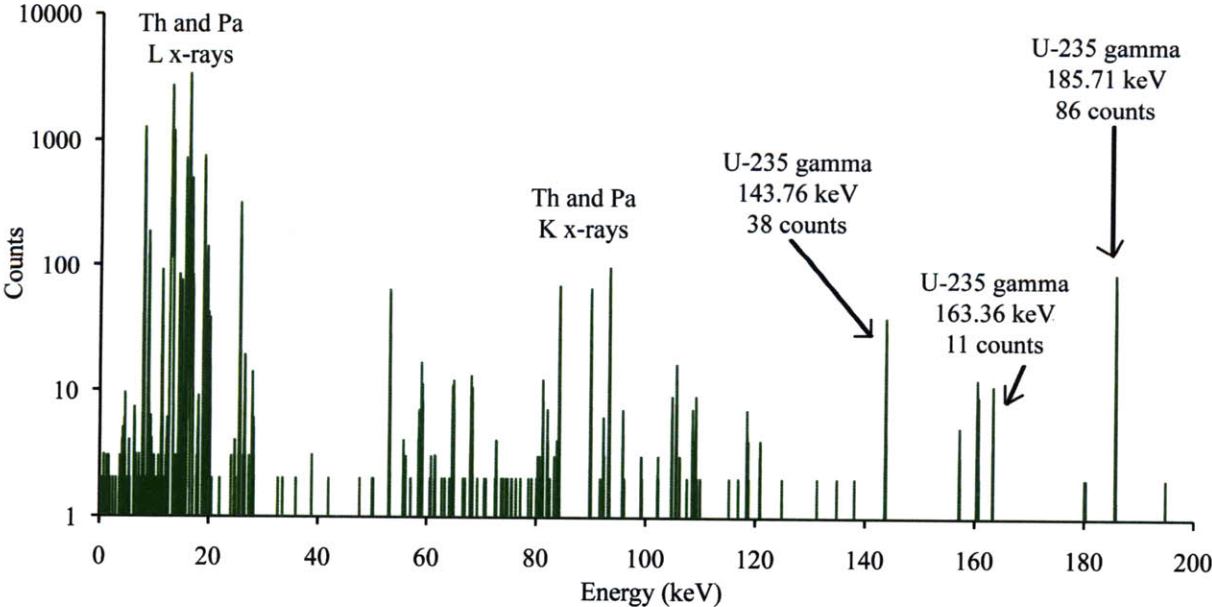


**Figure 11:** Simulation using RadSrc of weapons grade uranium incident on the detector with an inset focusing on the main U-235 gammas.

response of superconducting detectors. As seen in figure 11, there are some high intensity x-ray peaks at energies below 20 keV. The Th L lines are caused by the decay of U into Th and the Pa L x-rays accompany the decay of the Th isotopes into Pa. The K x-rays are not as intense, but are still visible at higher energies between 85 keV and 110 keV. Table 2 lists the most intense peaks caused by x-rays. The intensity of the Pa x-rays are comparable to those of Th because even if it is not a direct decay product of U-235, the half-life of Th-231 is only 25.52 hours. This means that Th-231 reaches secular equilibrium with U-235 quickly and rapidly transforms into Pa-231. The resolution offered by the superconducting detector model is high enough to identify each of the x-rays individually.

**Table 2:** Most intense peaks caused by thorium and protactinium x-rays from the decay of U-235 and Th-231, respectively.

Energy (keV)	Counts	X-ray	Energy (keV)	Counts	X-ray
12.8	1713	Th L <sub>α2</sub>	18.96	2985	Th L <sub>γ1</sub>
12.96	14541	Th L <sub>α1</sub>	19.3	52	Th L <sub>γ2</sub>
13.12	783	Pa L <sub>α2</sub>	19.5	48	Th L <sub>γ3</sub>
13.28	6476	Pa L <sub>α1</sub>	19.56	608	Pa L <sub>γ1</sub>
14.5	445	Th L <sub>h</sub>	19.88	203	Pa L <sub>γ2</sub>
14.96	230	Th L <sub>β6</sub>	20.1	191	Pa L <sub>γ3</sub>
15.6	3817	Th L <sub>β2</sub>	89.95	331	Th K <sub>α2</sub>
15.64	133	Th L <sub>β4</sub>	92.28	21	Pa K <sub>α2</sub>
16	1657	Pa L <sub>β2</sub>	93.34	479	Th K <sub>α1</sub>
16.2	17895	Th L <sub>β1</sub>	95.86	26	Pa K <sub>α1</sub>
16.42	71	Th L <sub>β3</sub>	104.81	48	Th K <sub>β3</sub>
16.7	2766	Pa L <sub>β1</sub>	105.6	77	Th K <sub>β1</sub>
16.92	441	Pa L <sub>β3</sub>	108.58	36	Th K <sub>β2</sub>

The most intense visible uranium gammas are due to the decay of U235 at 143.76 keV (I=10.96%), 185.71 keV (I=57.2%) and 163.36 keV (I=5.08 %). The less intense gamma rays at lower energies (20 – 60 keV) have a low count rate but are still discernable, as seen in figure 11, demonstrating that superconducting detectors can detect these low energy uranium lines.

## Analyzing Plutonium

Weapons grade plutonium is composed of mostly Pu-239 (see Appendix B), which has its strongest gammas at 38.66 keV, 51.62 keV and 129.29 keV, with comparably low branching ratios between 0.027% and 0.00631% even for these “strongest” lines. Pu-239 decays via alpha emission to U-235 with a half-life of 24,110 years. The low branching ratio, the comparably long half-life, and the small detector volume make the plutonium gammas intensities rather small, with the total number of counts below 10 for a total of 60 million simulated input particles. As seen in figure 12, the Pu-239 gammas are hard to make out when looking at the entire spectrum. Figure 13 takes the previous spectrum and zooms in on the graph by changing the range of the y-axis. This way the peaks of Pu-239 are recognizable. The background is quite low in these simulations and does not mask the Pu239.

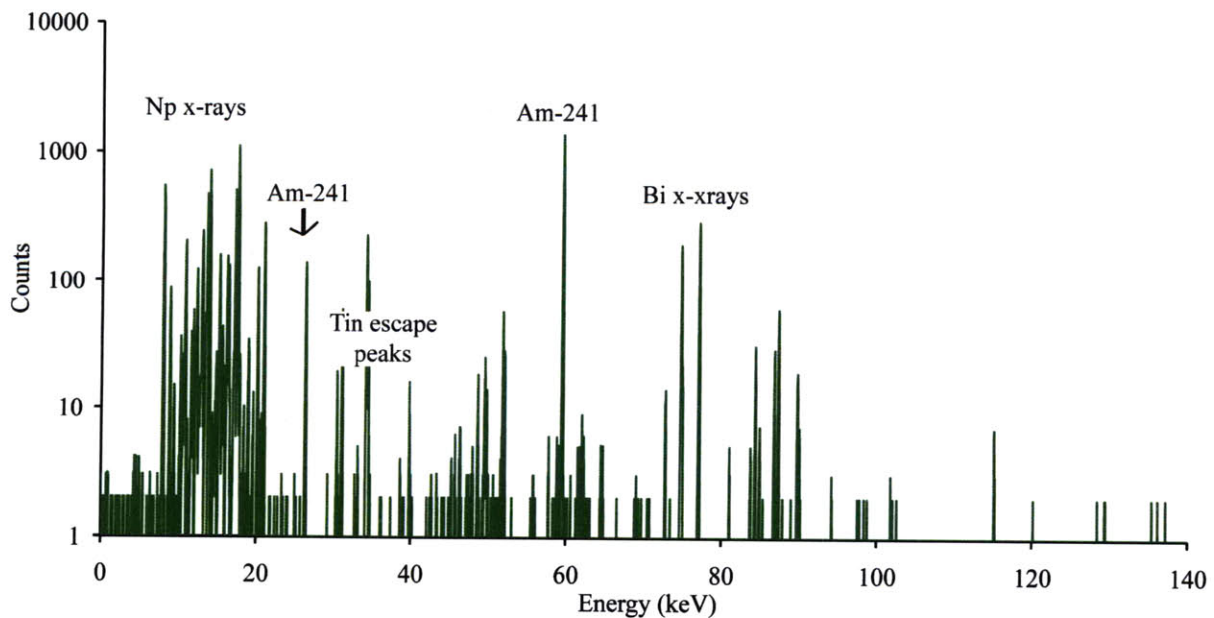
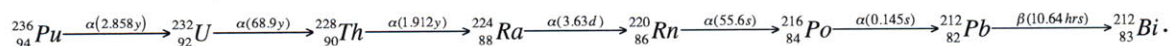


**Figure 12:** Simulation of a weapons grade plutonium source depicting the most intense gamma rays from Am-241, a decay product of Pu-241.

The highest peaks in the entire spectrum come from the decay of Pu-241 into Am-241, since its half-life is only 14.35 years and the branching ratio of the Am-241 line at 60 keV is 35.9%. Am-241 is also responsible for the strong gammas at 26.34 keV and the Np x-rays at 13.92 keV, 17.22 keV, 17.6 keV and 20.98 keV. The tin escape peaks are visible at 31 keV ( $K_{\beta}$ ), 34.26 keV ( $K_{\alpha 1}$ ) and 34.5 keV ( $K_{\alpha 2}$ ). The other strong lines at 10.82 keV, 74.8 keV and 77.1 keV come from the latter part of the plutonium decay chain, when lead decays into bismuth releasing intense Bi x-rays. The x-rays can be caused by the decay of Pu-236, Pu-238, Pu-240, Pu-242 or Pu-242; however the major contributor to the intensity is most likely Pu-236 since it has the shortest half-life (2.858 years). The decay chain is as follows:



The other visible medium sized peaks in the spectrum are the uranium x-rays.

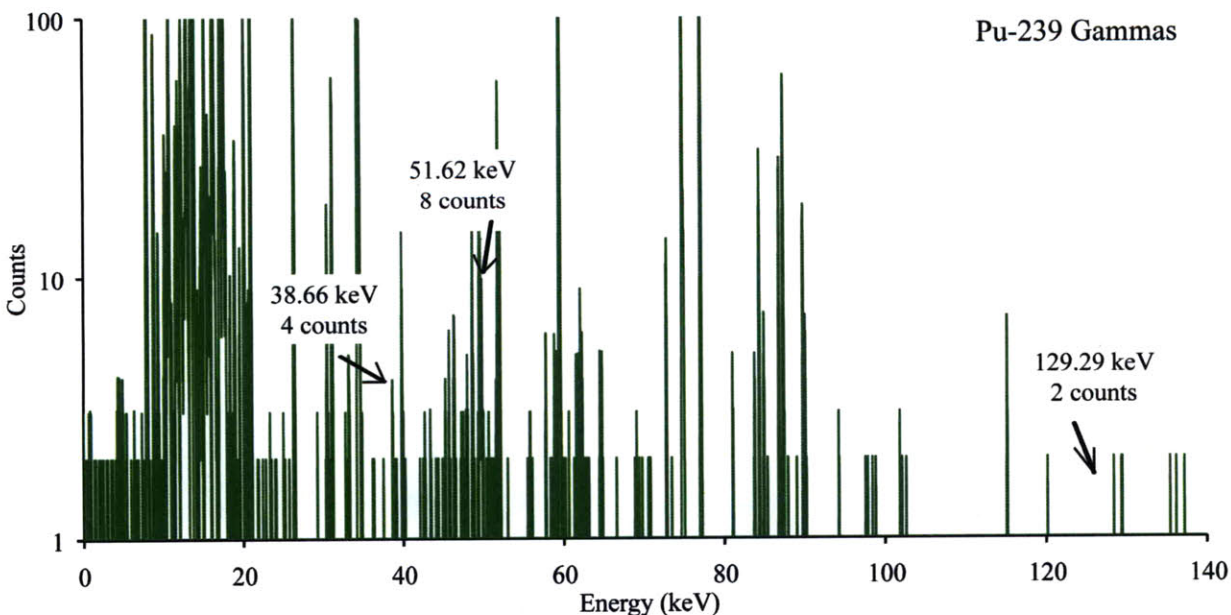


**Figure 13:** The same simulation of a weapons grade plutonium source as figure 12, scaling down the y-axis to focus on the Pu-239 gamma lines.

## Spent Fuel Examples

ORIGEN 2.1, a one-group depletion and radioactive decay computer code, is used to determine the isotopic composition of spent fuel emitted by three different reactor types: pressurized water reactor (PWR), a boiling water reactor (BWR) and a CANDU (“CANada Deuterium Uranium”) reactor. The spent fuel composition (detailed in Appendix B) was used as the initial input and aged by 30 years using RadSrc. The PWR was assumed to be a typical reactor using uranium fuel enriched 4.2% with U-235 and operating at 50 MWd/kgU. The uranium fuel for the BWR example was enriched 3.4% and assumed to be operating at 40 MWd/kgU. Finally the spent fuel for the CANDU is naturally enriched uranium from a reactor operating at 7.5 MWd/kgU. Since the spent fuel composition of each of the reactor types were fairly similar, in the sense that their radiation was dominated by the fission products, their

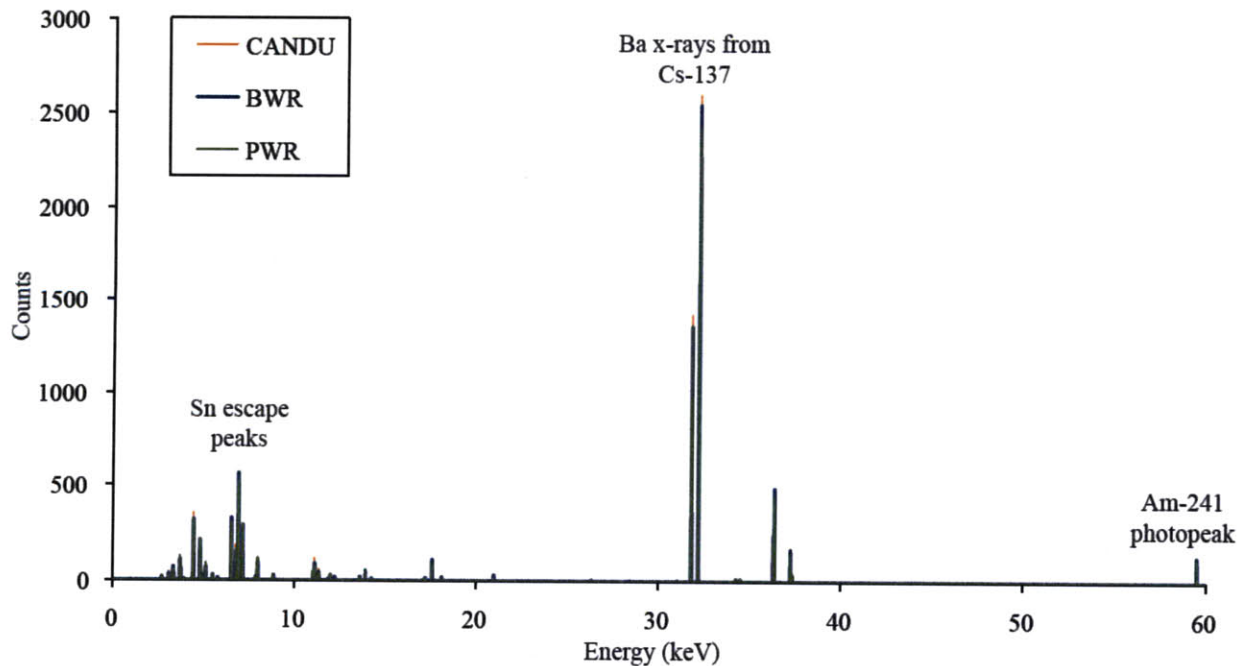


**Figure 14:** The energy spectra for a CANDU, BWR and PWR spent fuel source using the GEANT4 model. The most visible peaks are of one of the main fission products, Cs-137.

gamma spectra (figure 14) matched quite closely with a few differences in the number of counts.

The main peaks visible in the low-energy part of the spectrum are due to the fission products such as Cs-137, which produces barium x-rays when its decay to Ba-137. This happens because the half-life of Cs-137 is comparably short at 30.07 years and the percentage of Cs-137 in the initial spent fuel composition is relatively high at about 3% for the PWR and BWR. The medium sized peaks are attributed to Am-241 with a half-life of 432.2 years, significantly longer than Cs-137 but still much shorter than U-235's half-life of  $7.038 \times 10^8$  years. The lines for U-235 and Pu-239 are not visible in the simulation for a total number of 60 million input particles. The composition of the material was taken at the discharge value for the isotopes and aged 30 more years with RadSrc. This means that the spent fuel is still relatively fresh from the reactor and many of the strong fission product isotopes have not had time to decay. After 30 years, the Am-241 composition increased from 0.005359% to 0.124061%, due to the short half-life of Pu-241. On the other hand, the Cs-137 composition decreased by half from 3.89% to 1.94859%. If the simulation were to run even longer, the Cs-137 composition abundance will decrease, the intensity of the Cs-137 lines will decrease, and the other peaks will become more predominant, especially with the low background that superconducting detectors offer. Pu-239 and U-235 have really long half-lives and are therefore hard to detect after discharge. The superconducting detectors do offer a large increase in resolution and lower the background, but it appears that the fission products are still too intense for fresh spent fuel, at least for a comparably small number of 60 million total initial particles in the simulation. The next step in this research will be to significantly increase the total number of particles in the simulation and to extend the simulations to spent fuel composition that has aged for a longer time frame.

## CONCLUSION

Superconducting detectors are a promising technology for directly identifying fissile material in spent fuel in a non-destructive manner. The IAEA has several NDA safeguarding techniques based on gamma spectroscopy, but none of them are capable of directly identifying fissile isotopes in spent nuclear fuel. NaI, CdZnTe and HPGe detectors are efficient detectors to identify gamma rays emitted from the fission products of spent fuel. Nevertheless, they do not have a high enough energy resolution, nor a sufficiently high peak-to-background ratio to be able to identify the lower energy gammas from the fissile material in the presence of a large Compton background originating from the fission products. Superconducting detectors have the potential to identify these lower energy gammas from U-235 or Pu-239 that are often masked by the high background. This is possible because of their high resolution and the small size of the detector ( $\sim 1 \text{ mm}^3$ ) with a correspondingly small total Compton cross section for the high energy gammas. The inconveniences of these detectors include a limited dynamic range that depends on the transition of the detector between its normal and superconducting state, a low count-rate that leads to long analysis times, and the need to be cooled to 0.1 K that leads to a bulky spectrometer and a long cooldown time for the detector to be ready for use.

To analyze the capabilities of superconducting detectors, GEANT4 simulations were run initially using a 60 keV Am-241 source. The simulation matched the experimental data from a superconducting detector, therefore verifying the accuracy of the simulation. The simulation was also compared to experimental data from an HPGe detector and the benefits of a superconducting detector were clearly identified, namely the energy resolution of the TES and its peak-to-background ratio were significantly better. Small changes in the detector geometry can lead to

subtle but significant changes in the energy spectrum. When the dimensions of the absorber were changed while keeping the volume at  $1 \text{ mm}^3$ , it became apparent that the thinner the absorber the higher the photopeak with an increase in the peak-to-background ratio. This holds true as long as the absorber is thicker than the absorption length. The copper block behind the detector was changed to a copper ring and the backscatter peak decreased because there was less copper for the gammas to scatter from. The TES model can serve as a guide to improving superconducting detectors by understanding the contributions of the different parts to the energy spectrum.

The second set of simulations used RadSrc in combination with GEANT4 to run more complicated initial inputs. The first inputs used were for weapons grade uranium and plutonium. The highest peaks in the energy spectrum were for the decay products of U-235 and Pu-239, and for both of these models the main U-235 and Pu-239 gamma lines were visible within the spectrum. The direct detection of these lines can lead to a direct measure of the fissile content in the material. The next simulation consisted of spent fuel aged 30 years originating from a PWR, BWR and CANDU reactor. The results for all three spectra were very similar and the main peaks for both U-235 and Pu-239 were not visible for a total number of 60 million input particles. The highest peaks were due to the fission product Cs-137, because the half-life of Cs-137 is significantly lower than the half-life of the fissile content, and the branching ratio of the different lines is many orders of magnitude bigger than that of Pu, so that the Cs-137 emission is greater than  $10^7$  more intense than that of Pu. Superconducting detectors may have the ability to detect fissile material in spent fuel directly, but the total number of events in the simulation has to be increased significantly to find out. Alternatively, the sample could be aged more, so that the very strong fission gammas are not the only lines measured. Future simulations will repeat the spent fuel measurement with better statistics and with a composition that has been aged longer.



## ACKNOWLEDGMENTS

I would like to thank Stephan Friedrich and Richard Lanza for their excellent guidance and support. I would also like to acknowledge the technical support from Jonathan Dreyer and Owen Drury. I gratefully acknowledge the support of the NNSA Consortium Internship Program and of the Society of Professional Hispanic Engineers (SHPE). Finally I gratefully acknowledge the support of my parents, Monica Kahn, my fellow course 22 classmates and The Tech for making the past four years at MIT a life changing experience.

## REFERENCES

- [1] M.L. WALD (The New York Times), “Nuclear Energy,” Available on the internet at <http://www.nytimes.com/info/nuclear-energy/?scp=1-spot&sq=nuclear%20energy&st=cse> (May 10, 2010)
- [2] D. FISHER (International Atomic Energy Agency), “History of the IAEA,” Available on the internet at <http://www.iaea.org/About/history.html> (April 3, 2010).
- [3] C. SANG-HUN (The New York Times), “North Korea Claims to Conduct 2nd Nuclear Test,” Available on the internet at [http://www.nytimes.com/2009/05/25/world/asia/25nuke.html?\\_r=1](http://www.nytimes.com/2009/05/25/world/asia/25nuke.html?_r=1) (April 3, 2010).
- [4] D.E. SANGER, W.J. BROAD (The New York Times), “Agencies Suspect Iran is Planning Atomic Sites,” Available on the internet at <http://www.nytimes.com/2010/03/28/world/middleeast/28nuke.html> (April 3, 2010).
- [5] IAEA, “Safeguard Agreements and Additional Protocols,” Available on the internet at <http://www.iaea.org/OurWork/SV/Safeguards/sv.html> (April 5, 2010).
- [6] IAEA, “Safeguards Techniques and Equipment,” *International Nuclear Verification Series*, Vienna, Austria, No. 1 (Revised), IAEA (2003).
- [7] M. ZENDEL, M. MOESLINGER, “IAEA Safeguard Techniques,” *Advance Sensors for Safeguards*, Santa Fe, New Mexico, International Atomic Energy Agency (2007).
- [8] S.J. Luke, “Passive and Active Interrogation Method,” *NGSI Summer Lecture Series*, Livermore, California, Lawrence Livermore National Laboratory (2009).
- [9] S. FRIEDRICH, S.F. TERRACO, T. MIYAZAKI, O.B. DRURY, Z.A. ALI, M.F. CUNNINGHAM, “Design of a Multi-Channel Ultra-High Resolution Superconducting Gamma-Ray Spectrometer,” *Proc. SPIE*, Vol. 5540, pp. 156-164 SPIE (2004).

- [10] S.H. MOSELEY, J.C. MATHER, D. MCCAMMON, "Thermal Detectors as X-ray Spectrometers," *J. Appl. Phys.*, Vol. 56, pp. 1257-1262 (1984).
- [11] W.B. DORIESE, J.N. ULLOM, J.A. BEALL, W.D. DUNCAN, L. FERREIRA, G.C. HILTON, R.D. HORANSKY, K.D. IRWIN, J.A.B. MATES, C.D. REINTSEMA, L.R. VALE, Y. XU, B.L. ZINK, "14-pixel, multiplexed array of gamma-ray microcalorimeters with 47 eV energy resolution at 103 keV," National Institute of Standards and Technology (2007).
- [12] J.M. BRAKE, J.F. BURGER, H.J. HOLLAND, J.H. DERKING, H. ROGALLA, "Micromachined Cryogenic Coolers for Cooling Low-Temperature Detectors and Electronics," University of Twente (2010).
- [13] S.F. TERRACOL, S. ALI, T.R. NIEDERMAYR, I.D. HAU, O.B. DRURY, Z.A. Ali, T. MIYAZAKI, M.F. CUNNINGHAM, J.G. DREYER, J.D. LEACOCK, S. FRIEDRICH, "Ultra-High Resolution Gamma ray Spectrometer Development for Nuclear Attribution and Non-Proliferation Applications," Lawrence Livermore National Laboratory (2004).
- [14] J.R. PHILLIPS & D. REILLEY, N. ENSSLIN, H. SMITH, S. KREINER (Eds.), "Irradiated Fuel Measurements," *Passive Nondestructive Assay Manual*, pp. 529-562 (1991).
- [15] A.D. DOUGAN, "Grand Challenges for Safeguards," *Next Generation Safeguards Initiatives Summer Lecture Series*, Livermore, California, Lawrence Livermore National Laboratory (2009).
- [16] S. AGOSTINELLI, et al. (Geant4 collaboration), "Geant4 User's Guided for Application Developers, Version: geant4 9.2," Available on the Internet at <http://geant4.web.cern.ch/geant4/UserDocumentation/UsersGuides/ForApplicationDeveloper/html/> (October 1, 2009).
- [17] G.F. KNOLL, *Radiation Detection and Measurement*, 3rd Ed., John Wiley & Sons (2000).
- [18] L. HILLER, T. GOSNELL, J. GRONBER, D. WRIGHT, "RadSrc/Monte Carlo Code Interface Manual," Lawrence Livermore National Laboratory (2007).

## APPENDIX A

**Table 2.7**

**STATES WITH SIGNIFICANT NUCLEAR ACTIVITIES AS AT THE END OF 2005, 2006, 2007**

	Number of States		
	2005	2006	2007
States with safeguards applied under INFCIRC/153-type agreements:	64	65	64 <sup>a/ b/</sup>
• States with additional protocols in force (or otherwise applied)	45	45	47 <sup>a/</sup>
States with safeguards applied under INFCIRC/66-type agreements	3	3	3
States with voluntary offer agreements in force	5	5	5
<b>Total number of States<sup>a/</sup> with significant nuclear activities</b>	<b>72</b>	<b>73</b>	<b>72<sup>a/ b/</sup></b>

a/ Safeguards, including the measures under the Model Additional Protocol, were also applied in Taiwan, China.

b/ DPRK is not included.

Source: IAEA, "Safeguard Agreements and Additional Protocols," Available on the internet at <http://www.iaea.org/OurWork/SV/Safeguards/sv.html> (April 5, 2010).

Table A5. Number of facilities under safeguards or containing safeguarded material on 31 December 2008

Facility type	Number of facilities			Total
	Comprehensive safeguards agreements <sup>a</sup>	INFCIRC/66 <sup>b</sup> type agreements	Voluntary offer agreements	
Power reactors	226	5	1	232
Research reactors and critical assemblies	151	4	1	156
Conversion plants	20	0	0	20
Fuel fabrication plants	42	3	1	46
Reprocessing plants	11	1	1	13
Enrichment plants	13	0	3	16
Separate storage facilities	111	2	6	119
Other facilities	84	0	0	84
<b>Subtotals</b>	<b>659</b>	<b>14</b>	<b>13</b>	<b>686</b>
Other locations	444	1	0	445
<b>Totals</b>	<b>1103</b>	<b>15</b>	<b>13</b>	<b>1131</b>

<sup>a</sup> Covering safeguards agreements pursuant to the NPT and/or the Treaty of Tlatelolco and other CSAs; includes facilities in Taiwan, China.

<sup>b</sup> Covering facilities in India, Israel and Pakistan.

Source: IAEA, "Safeguard Agreements and Additional Protocols," Available on the internet at <http://www.iaea.org/OurWork/SV/Safeguards/sv.html> (April 5, 2010).

Table A4. Approximate quantities of material subject to Agency safeguards at the end of 2008

Type of material	Quantity of material (SQs) <sup>a</sup>			Quantity in SQs
	Comprehensive safeguards agreements <sup>b</sup>	INFCIRC/66 <sup>c</sup> type agreement	Voluntary offer agreements	
<b>Nuclear material</b>				
Plutonium <sup>d</sup> contained in irradiated fuel and in fuel elements in reactor cores	105 657	1 070	15 154	121 881
Separated plutonium outside reactor cores	1 429	5	10 009	11 443
HEU (equal to or greater than 20% <sup>235</sup> U)	267	1	49	317
LEU (less than 20% <sup>235</sup> U)	15 006	146	795	15 947
Source material <sup>e</sup> (natural and depleted uranium and thorium)	7 576	108	1 379	9 063
U-233	19	—	—	19
<b>Total significant quantities</b>	<b>129 954</b>	<b>1 330</b>	<b>27 386</b>	<b>158 670</b>
<b>Non-nuclear material<sup>f</sup></b>				
Heavy water (tonnes)	0.7	449.3	—	—

<sup>a</sup> SQ: significant quantity. Defined as the approximate amount of nuclear material for which the possibility of manufacturing a nuclear explosive device cannot be excluded. Significant quantities take into account unavoidable losses due to conversion and manufacturing processes and should not be confused with critical masses. They are used in establishing the quantity component of the Agency's inspection goal.

<sup>b</sup> Covering safeguards agreements pursuant to the NPT and/or the Treaty of Tlatelolco and other CSAs; includes facilities in Taiwan, China.

<sup>c</sup> Covering facilities in India, Israel and Pakistan.

<sup>d</sup> The quantity includes an estimated 11 520 SQs of plutonium in irradiated fuel, which is not yet reported to the Agency under the reporting procedures agreed to (the non-reported plutonium is contained in irradiated fuel assemblies to which item accountability and containment/surveillance measures are applied), and plutonium in fuel elements loaded into cores.

<sup>e</sup> This table does not include material within the terms of subparagraphs 34(a) and (b) of INFCIRC/153 (Corrected).

<sup>f</sup> Non-nuclear material subject to Agency safeguards under INFCIRC/66/Rev.2 type agreements.

Source: IAEA, "Safeguard Agreements and Additional Protocols," Available on the internet at <http://www.iaea.org/OurWork/SV/Safeguards/sv.html> (April 5, 2010).

## APPENDIX B

Different RadSrc inputs:

	Purpose	Input		
Aged Uranium	Good for unknown sources- compare count rate at different ages → Weapons Grade Uranium	U235 93.5 U238 5.5 U234 1.0 AGE 30 50 100 150 200		
Plutonium	Analyze the response of the low energy gammas. → Weapons grade plutonium	Pu239 93.5 Pu240 6.0 Pu241 0.44 Pu236 0.02 Pu244 0.02 Pu242 0.015 Pu238 0.005 AGE 30		
Spent Fuel	Energy Spectrum of Spent Fuel from Different Reactor Types	PWR-4.2% 50MWd/kg	U233	4.572E-08
			U234	0.0003642
			U235	0.6569
			U236	0.5486
			U237	0.001922
			U238	92.23
			NP237	0.09171
			NP239	0.01066
			PU238	0.03917
			PU239	0.6794
			PU240	0.3228
			PU241	0.1604
			PU242	0.07205
			AM241	0.005359
			AM243	0.02104
			CM244	0.01044
			CM245	0.0005465
			CS137	3.89
			BA137	1.2586383
			TH230	1.06E-09
			TH232	3.605E-08
			PA231	1.895E-09
		BWR-3.4% 40MWd/kg	U233	3.616E-08
			U234	0.0002449

			U235	0.7219
			U236	0.4388
			U237	0.001629
			U238	93.5
			NP237	0.06812
			NP239	0.0105
			PU238	0.02841
			PU239	0.592
			PU240	0.2485
			PU241	0.1673
			PU242	0.06707
			AM241	0.004741
			AM243	0.01921
			CM244	0.008942
			CM245	0.0004787
			BA137	0.976354339
			CS137	3.1458
			PA231	1.509E-09
			TH230	6.089E-10
			TH232	2.278E-08
		CANDU- 0.7% 7.5MWd/kg	TH230	2.104E-12
			TH232	5.181E-10
			PA231	1.797E-10
			U233	1.208E-09
			U234	0.00002623
			U235	0.3151
			U236	0.0582
			U237	0.0001214
			U238	98.78
			NP237	0.001572
			NP239	0.008563
			PU238	0.0001372
			PU239	0.2345
			PU240	0.06364
			PU241	0.01084
			PU242	0.00169
			AM241	0.00007268
			AM242M	3.462E-07
			AM242	3.106E-07
			AM243	0.00003804
			CM244	0.00002032
		CM245	1.226E-08	
		CS137	0.525399754	
		BA137	0.0001206	